PERGAMON

International Journal of Heat and Mass Transfer 42 (1999) 1157–1175

International Journal of HEAT and MASS TRANSFER

# Investigation of the cooling of hot walls by liquid water sprays

Michele Ciofalo[a,*], Ivan Di Piazza[a], Valerio Brucato[b]

[a] *Dipartimento di Ingegneria Nucleare, Università di Palermo, Viale delle Scienze, 90128 Palermo, Italy*
[b] *Dipartimento di Ingegneria Chimica dei Processi e dei Materiali, Università di Palermo, Viale delle Scienze, 90128 Palermo, Italy*

Received 20 November 1997; in final form 6 August 1998

**Abstract**

An experimental study was conducted for the heat transfer from hot walls to liquid water sprays. Four full cone, swirl spray nozzles were used at different upstream pressures, giving mass fluxes impinging on the wall, $G$, from 8 to 80 kg $m^{-2}$ $s^{-1}$, mean droplet velocities, $U$, from 13 to 28 m $s^{-1}$ and mean droplet diameters, $D$, from 0.4 to 2.2 mm.

A target consisting of two slabs of beryllium–copper alloy, each $4 \times 5$ cm in size and 1.1 mm thick, was electrically heated to about 300°C and then rapidly and symmetrically cooled by water sprays issuing from two identical nozzles. The midplane temperature was measured by a fast response, thin-foil thermocouple and the experimental data were regularized by Gaussian filtering.

The inverse heat conduction problem was then solved by an approximation of the exact Stefan solution to yield the wall temperature $T_w$ and the heat flux $q_w$ transferred to the spray at temperature $T_f$. As a result, cooling curves expressing the heat flux $q_w$ as a function of $T_w - T_f$ were obtained. The single-phase heat transfer coefficient $h$ and the maximum heat flux $q_c$ were found to depend upon the mass flux $G$ and the droplet velocity $U$, while the droplet size $D$ had a negligible independent influence. Simple correlations for $h$ and $q_c$ were proposed. 

*Key words:* Spray cooling; Boiling heat transfer; Inverse heat conduction problem

**Nomenclature**

$A$ cross-sectional area of the spray at impact, $\pi(Xtg\theta)^2$ [$m^2$]
$A_0$ nozzle outlet area [$m^2$]
$Bi$ Biot number, $h\delta/\lambda_s$
$c_p$ specific heat at constant pressure [J $kg^{-1}$ $K^{-1}$]
$d$, $D$ generic and mean droplet diameter [m]
$F$ mass flow peaking factor, $GA/\dot{m}$
$G$ mass flux at spray center [kg $m^{-2}$ $s^{-1}$]
$h$ single-phase heat transfer coefficient, $q_w/(T_w - T_f)$ [W $m^{-2}$ $K^{-1}$]
$\dot{m}$ total mass flow rate [kg $s^{-1}$]
$p$ pressure [N $m^{-2}$]
$q$ heat flux [W $m^{-2}$]
$t$ time [s]
$T$ temperature [K]
$u$, $U$ generic and mean droplet velocity [m $s^{-1}$]
$x$ direction normal to wall and out of it [m]
$X$ nozzle–target distance [m]
$y$ smoothed midplane temperature [K].

*Greek symbols*

$\alpha$ thermal diffusivity, $\lambda/(\rho c_p)$ [$m^{-2}$ $s^{-1}$]
$\delta$ sample half-thickness [m]
$\theta$ half-opening angle of the spray cone [rad]
$\lambda$ thermal conductivity [W $m^{-1}$ $K^{-1}$]
$\rho$ density [kg $m^{-3}$]
$\tau$ conduction time constant, $\delta^2/\alpha$ [s]
$\tau^*$ convection time constant, function of $\tau$ and $Bi$ [s].

*Subscripts*

c critical
d droplet
DNB departure from nucleate boiling

* Corresponding author. Tel.: +39 91 232 257; fax: +39 91 232 215; e-mail: ciofalo@din.din.unipa.it

0017–9310/98/$ - see front matter 
PII: S0017–9310(98)00250–6

f fluid [water]
s solid
sat saturation
w wall.

## 1. Introduction

Cooling hot surfaces by liquid sprays is a very effective process, which may provide heat fluxes in excess of $10^7$ W/m$^2$, and thus is widely used in many industrial fields like metallurgy [1], microelectronics [2], nuclear safety [3] and aerospace engineering [4].

Experimental techniques used for heat measurements can be classified in two categories: steady state and transient methods.

In steady state experiments, heat transfer rates are derived from a thermal balance between the (usually electric) power input into an appropriate sample and the heat transferred to the spray. Measurements are conducted over times which are large compared to the time constants of the system. The application of steady state techniques is severely limited by the maximum attainable power densities; for example, a $4 \times 5$ cm metal slab cooled from both sides by a heat flux of $10^7$ W/m$^2$ would require an electric power of 40 kW to be kept at a constant temperature! Moreover, in power-controlled systems it is practically impossible to maintain steady state conditions in the unstable region of the heat transfer curve (transitional, or partial film, boiling). Because of these limitations, steady state methods have usually been confined to investigations involving low heat transfer rates.

In transient experiments, the target is typically heated to a uniform high temperature and then rapidly cooled by the spray while the temperatures at one or more locations within the sample are recorded. The surface heat flux and temperature can be calculated from the raw experimental data by various methods, usually involving smoothing and solving an inverse heat conduction problem. Transient techniques are the only viable ones when large heat flow rates are involved, and thus have been most commonly employed in real-scale spray cooling research.

Transient spray cooling tests are usually conducted under the assumption that, despite the time-dependent conditions of the measurements, the relation between wall temperature and wall heat transfer rates is the same that would be observed under steady state conditions. This is justified by the fact that the time constants characterizing the impact, spreading and vaporization of an individual droplet are usually much smaller than the time constants of the overall cooling transient.

For any given fluid the measured heat transfer rate is a function of wall and fluid temperatures, local spray mass flux $G$, droplet velocity $U$ and size $D$, and nature and finishing of the cooled surface. An extensive review of theoretical and experimental results for liquid spray cooling up to the late Seventies is given, for example, by Bolle and Moreau [5].

More recently, Choi and Yao [6] studied heat transfer to horizontal sprays. Typical values of the hydrodynamic parameters were $G = 0.3$–$2$ kg m$^{-2}$ s$^{-1}$, $U = 3$–$4$ m s$^{-1}$ and $D = 0.5$ mm. Maximum heat fluxes of up to $2 \times 10^6$ W m$^{-2}$ were measured for wall temperatures of $\sim$140–160°C, while the Leidenfrost point temperature was about 250°C. The influence of air flow on heat transfer in pneumatic sprays was also discussed.

Bernardin et al. [7] assessed the influence of surface roughness on water droplet impact history and heat transfer regimes; they also presented high quality photographic records of the droplet spreading, taken at 1 ms intervals. In this study, a single stream of droplets was produced; the mass flux did not exceed a fraction of kg m$^{-2}$ s$^{-1}$, yielding maximum cooling rates of the order of $10^2$°C s$^{-1}$ and maximum heat fluxes well below $1 \times 10^6$ W m$^{-2}$. The maximum heat flux was attained at temperatures of 105–110°C, while the Leidenfrost point temperature varied between 150–200°C. In a subsequent paper [8], the same authors presented more detailed results for droplets impacting on a polished surface and discussed the features of the boiling curve and the way of obtaining it from time-temperature series.

In both the above studies, the Biot number was well below one, so that the target could be assumed to be isothermal at each instant (cooling transients typically lasted more than 30 s), and no inverse heat conduction problem had to be solved.

Similar remarks hold for the work of Sawyer et al. [9], who also considered a single stream of droplets and presented a correlation for the critical heat flux as a function of the droplet Weber number and Strouhal number (dimensionless impact frequency). The mass flux did not exceed 1–2 kg m$^{-2}$ s$^{-1}$; maximum heat fluxes were found to be of the order of $5 \times 10^6$ W m$^{-2}$ once adjusted for the actual wetted area after droplet spreading, and were attained at wall temperatures of only $\sim$120°C.

On the whole, most of the experimental studies presented so far have focused on relatively low mass flow rates or on the film boiling heat transfer regime (wall temperature above the Leidenfrost point $T_L$), while data on nucleate boiling and single-phase heat transfer at high mass flow rates are comparatively scarce.

On the contrary, the present investigation focused on the latter conditions; mass fluxes up to 80 kg m$^{-2}$ s$^{-1}$ were considered, giving wall heat fluxes in excess of $10^7$ W m$^{-2}$ and cooling rates above $10^3$°C s$^{-1}$, while the wall temperature never exceeded 250–270°C (which, according to the above literature results, is close to the typical value of the Leidenfrost point temperature). The study was motivated by previous research on the influence of rapid cooling on the structure and properties of polymeric films [10], a subject of importance in connection with the injection moulding of macromolecular materials.

## 2. Hydrodynamic characterization of the sprays

The water sprays considered in the present investigation were generated by full-cone, swirl-spray pressure nozzles of the TG series, manufactured by Spraying System Co. The principle of a TG nozzle and a typical droplet impact pattern are sketched in Fig. 1.

From the hydrodynamic point of view, neglecting variables which are believed to play a minor role (such as the spatial distribution of the droplets), the main quantities which characterize locally a spray impacting on a surface are:

— the mass flux of the spray in the impact area, $G$;
— the droplet speed $u$ (and its distribution);
— the droplet diameter $d$ (and its distribution).

These quantities can be made to vary in a wide range by changing the nozzle geometry, the pressure drop $\Delta p$ across the nozzle and the nozzle to target distance $X$.

For the given fluid, ambient pressure and temperature of the hot surface, the only other parameters which may affect heat transfer are the degree of subcooling of the liquid, i.e., its temperature $T_f$, and the surface properties of the target.

In the present heat transfer measurements, four different nozzles were tested (TG1, TG2, TG5 and TG10), characterized by increasing values of the cross-sectional area and thus of the flow rate obtained for any given pressure drop.

Prior to heat transfer measurements, a separate study was conducted in order to characterize the behaviour of the hydrodynamic impact parameters $G$, $u$, $d$ for the different nozzles as functions of $\Delta p$ and $X$ [11]. The device used to generate the sprays is sketched in Fig. 2. An air compressor was adopted to pressurize up to 10 bar the water contained in a 24-l vessel. A large flexible pipe, 1 in (2.54 cm) in diameter, connected the vessel to the nozzle. Pressure could be read at different points of the rig; in particular, it was measured immediately upstream of the nozzle (manometre M2) to obtain the pressure drop across the nozzle, $\Delta p$. The same device, with the modifications which will be described in Section 3, was used in the heat transfer tests.

First, the total mass flow $\dot{m}$ for any given nozzle and for a given upstream pressure was assessed by simply measuring the volume of water discharged into a vessel in a given time (30 or 60 s). Results are summarized in Fig. 3(a); they lie very close to the theoretical law:

$$\dot{m} = C_q A_0 (2\rho\Delta p)^{1/2} \quad (1)$$

The discharge coefficient $C_q$ (computed on the basis of the nozzle outlet area provided by the manufacturer) was 0.68, 0.80, 0.52 and 0.64 for the nozzles TG1, TG2, TG5 and TG10, respectively.

The mass flux $G$ in the central region of the spray for a nozzle-target distance $X$ of 50 mm (the same at which the heat transfer tests were subsequently conducted) was measured by simply collecting the water crossing in a given time a circular opening 10 mm in radius (the reason for this choice is better discussed in Section 6). It is reasonable to assume that $G$ varies very little in the central region of the spray, corresponding to a half-opening angle of only $\sim 10^\circ$.

Results are summarized in Fig. 3(b). The behavior of $G$ is a consequence of the simultaneous variation of the spray cone half-opening angle $\theta$ and of the mass flow

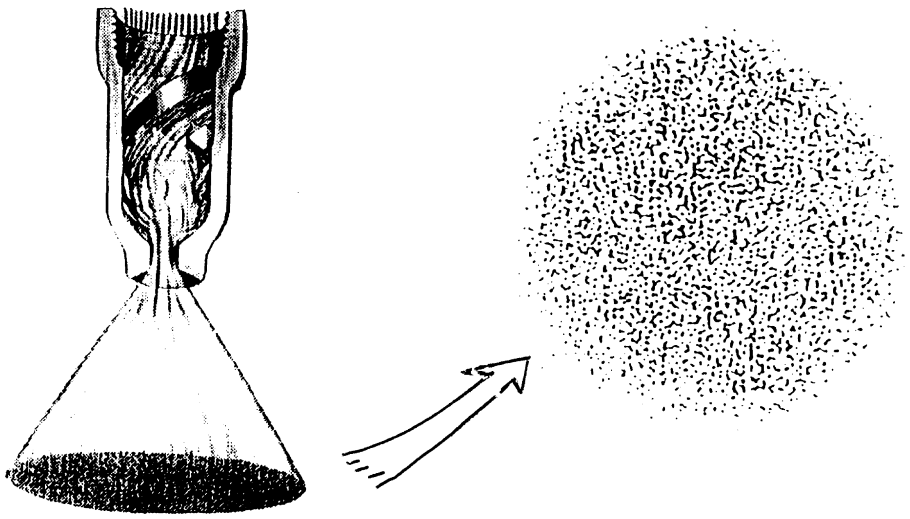

Fig. 1. Principle and typical droplet impact pattern of a TG-series swirl-spray nozzle.

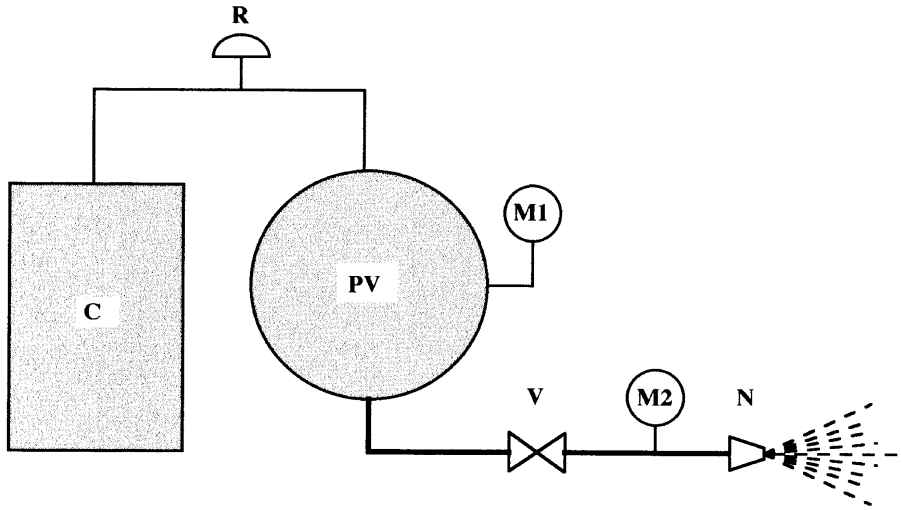


Fig. 2. Experimental setup for the characterization of the sprays. C: air compressor; PV: water-filled pressure vessel; M1, M2: manometers; R: pressure regulation valve; V: fast opening valve; N: nozzle.

peaking factor $F$ with $\Delta p$. In the pressure range examined ($\Delta p = 2$–8 bar), $\theta$ goes through a maximum at about 3–4 bar while $F$ decreases monotonically with increasing $\Delta p$, as was qualitatively confirmed by visual inspection of the marks left by the impacting droplets on a surface covered with a soft paste. In the limited range $\Delta p = 2$–8 bar considered here, the behaviour of $G$ with $\Delta p$ can be fairly well approximated as a linear dependence.

The velocity of the droplets was assessed by measuring the length of the tracks on still-frame video recordings of the sprays. Fast exposure times (1/500–1/1000th s, as controlled to $\pm 1\%$ by an electronic shutter) were used, so that tracks 20–40 mm in length (real size) were obtained for typical droplet speeds of 15–30 m/s. The sprays were illuminated by a 1000 W lamp equipped with a double slit collimator, which generated a 2 mm thick light sheet containing the spray axis and orthogonal to the optical axis of the camera. Only the droplets close to the spray axis and 5–10 cm apart from the nozzle exit were considered, so as to reproduce the conditions of the droplets impacting on the target during the subsequent thermal measurements. In these tests, a modest amount ($\sim 1\%$) of milk was added to the water in order to enhance the contrast of the droplet track images.

A large number of tracks (about a hundred) were measured for each combination of nozzle type and upstream pressure. Two typical resulting velocity distributions are shown in Fig. 4(a); they are roughly Gaussian, with a standard deviation ranging from 5–10% of the mean value, according to the specific nozzle.

The mean velocities $U$ computed from such distributions are reported in Fig. 4(b) as functions of the pressure drop $\Delta p$ for all four nozzles. Of course, they are somewhat lower than the theoretical efflux velocity:

$$U = (2\Delta p/\rho)^{1/2} \tag{2}$$

The velocity defect increases with increasing $\Delta p$, i.e., with increasing exit turbulence level; among the different nozzles, the largest deviations are observed for TG10, the smallest for TG5.

As regards the droplet diameter, in a spray it is not unique, but is rather a random variable which is often assumed to follow a log–normal distribution. Unfortunately, the accurate experimental determination of the droplet size distribution is a complex task, involving either the direct examination of photographic/video recordings of the spray or indirect optical techniques based on laser scattering and laser interferometry [5]. None of these methods was available in the present study.

For the Spraying System nozzles used in the present study, the manufacturer provides the mean volume diameter MVD, measured by small-angle light scattering, as a function of the nozzle type and of the upstream pressure; data are reported in Fig. 5. The quantity MVD is defined so that half the spray volume is contained in droplets of diameter less than MVD, and half in larger droplets; it does not coincide with the diameter of droplets having the average volume, but rather is related to this, more conventional, quantity in a complex way which depends on the exact statistical distribution of the droplet sizes. In this study, MVD was identified to all practical purposes with the mean diameter $D$ of the droplets.

Figure 5 shows that MVD decreases with increasing pressure drop (i.e., flow rate) and varies considerably

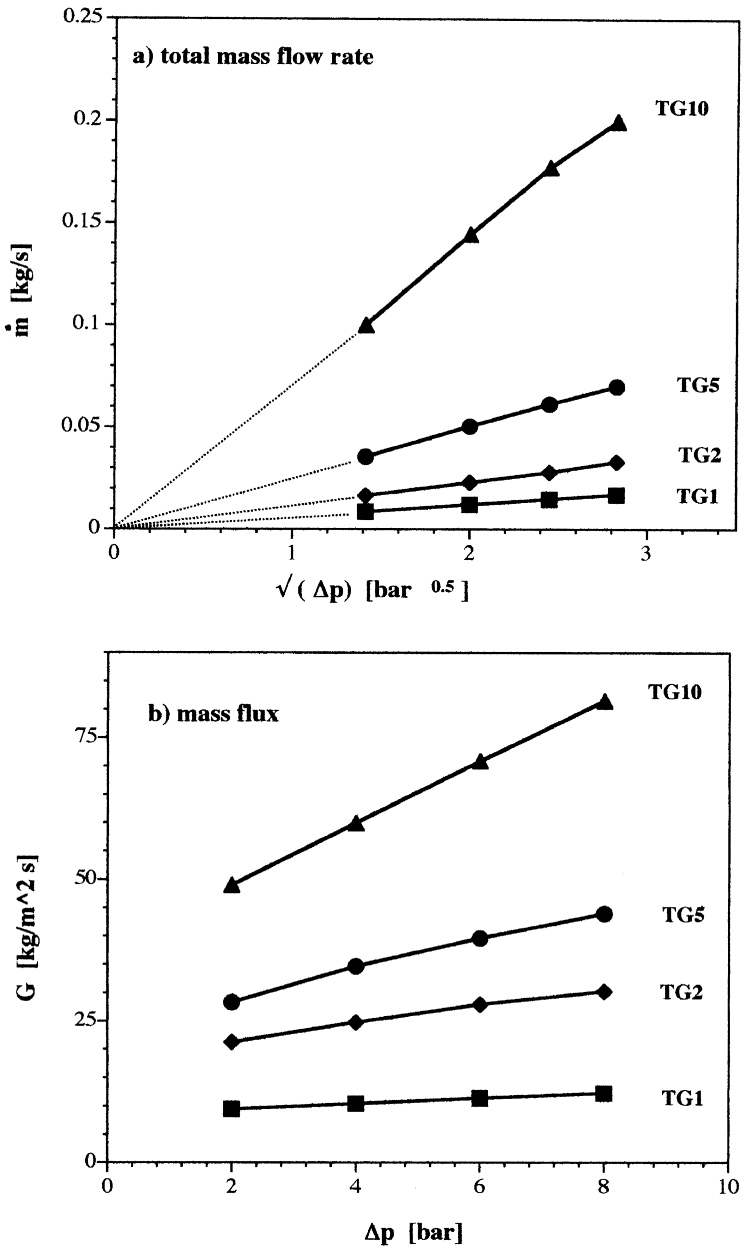


Fig. 3. Results of the flow rate measurements. Total mass flow rate (a) and centerline specific mass flow rate at 50 mm (b) as functions of the pressure drop for all nozzles.

among the different nozzles. In the present study, the droplet diameter ranged from ~0.4 mm (nozzle TG1, $\Delta p = 8$ bar) to ~2.2 mm (nozzle TG10, $\Delta p = 2$ bar).

The correlation between droplet diameter and droplet speed, as well as other aspects of the interaction between droplets and between droplets and air, are complex phenomena which could not be investigated in the present study. However, at the short distance from the nozzle outlet considered here (50 mm, i.e., from 23 to 125$D$), in the authors' opinion, very little size-dependent velocity scatter is to be expected in the spray.

## 3. Heat transfer measurements

The target used in the present study, Fig 6(a), consisted of two identical slabs of copper-beryllium ($\rho = 8250$ kg

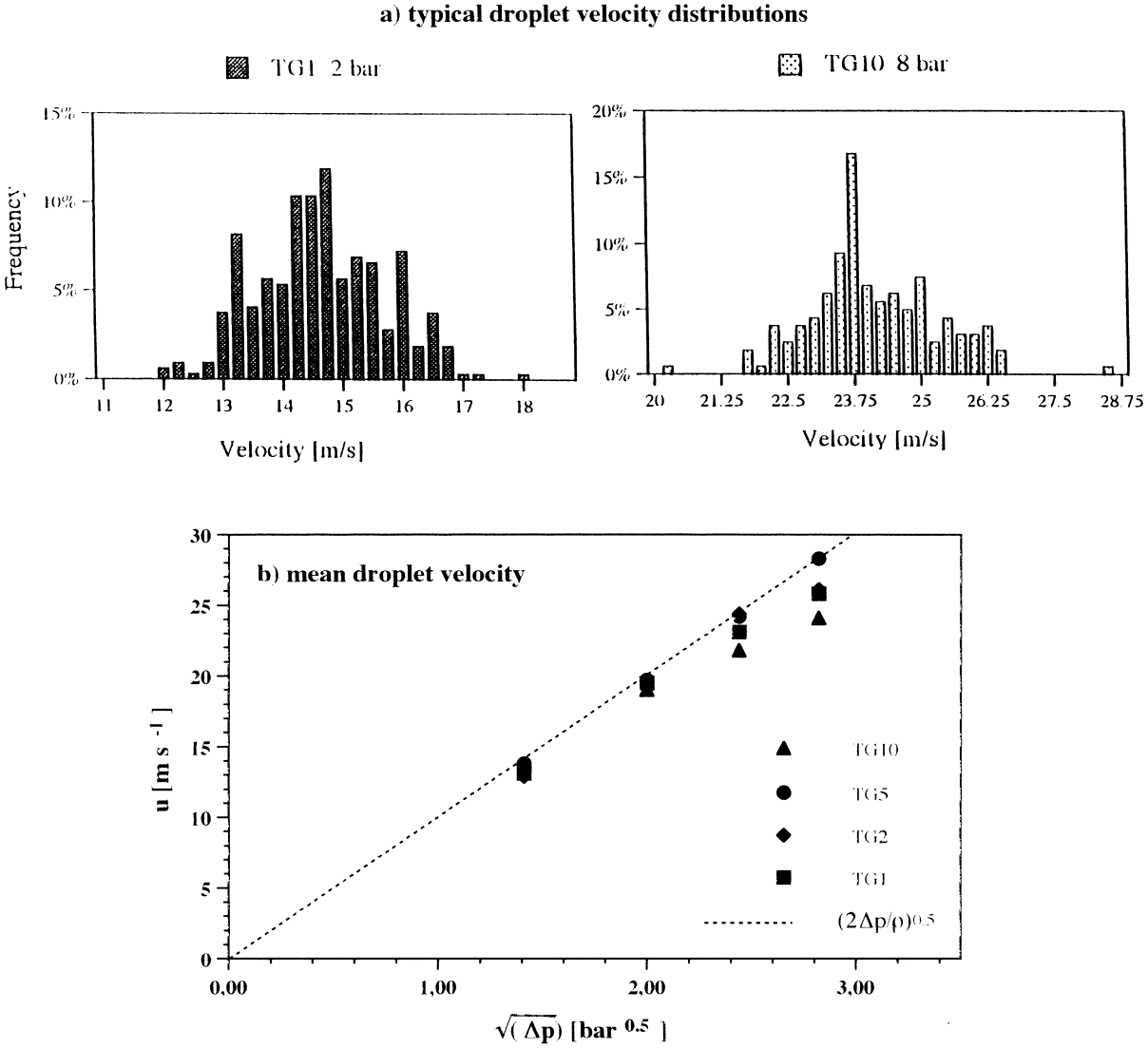


Fig. 4. Results of the droplet velocity measurements: (a) typical droplet velocity distributions; (b) mean droplet velocity as a function of the pressure drop for all nozzles.

$m^{-3}$, $c_p = 415\ J\ kg^{-1}$, $\lambda = 100\ W\ m^{-1}\ K^{-1}$), each $40 \times 50$ mm in size and 1.1 mm in thickness, tightly pressed together by steel springs. The intrinsic time constant of the target, $(4/\pi^2)\ \delta^2/\alpha$, was $\sim 16 \times 10^{-3}$ s. For a typical heat transfer coefficient $h$ to the spray of $\sim 50000\ W\ m^{-2}\ K^{-1}$, the Biot number $h\delta/\lambda$ was $\sim 0.5$ and the overall cooling time constant was of the order of 0.1 s [12].

A thin-foil copper-constantan thermocouple (Omega 'cement on—style II' type) was sandwiched between the two slabs at the center of the target. Its junction, some $1 \times 2$ mm in lateral size, had a thickness of only 1/2 mils ($\sim 13\ \mu m$) and thus a negligible intrinsic time constant. In order both to insulate it electrically from the slabs—thus reducing noise in the signal—and also to protect it mechanically, the thermocouple was wrapped in a thin Teflon foil, some 5 $\mu$m in thickness. The overall conductive time constant of the package was estimated to be only a few ms, i.e., far less than the characteristic time constants of the cooling transients.

The device used for the heat transfer measurements is sketched in Fig. 6(b). The target, mounted on a sliding frame, was first brought to a uniform temperature (typically $\sim 300°C$) by thermal radiation from a cluster of nichrome resistance heaters, disposed symmetrically on both sides of the target and at a distance of a few mm from it. Once the required steady-state conditions were

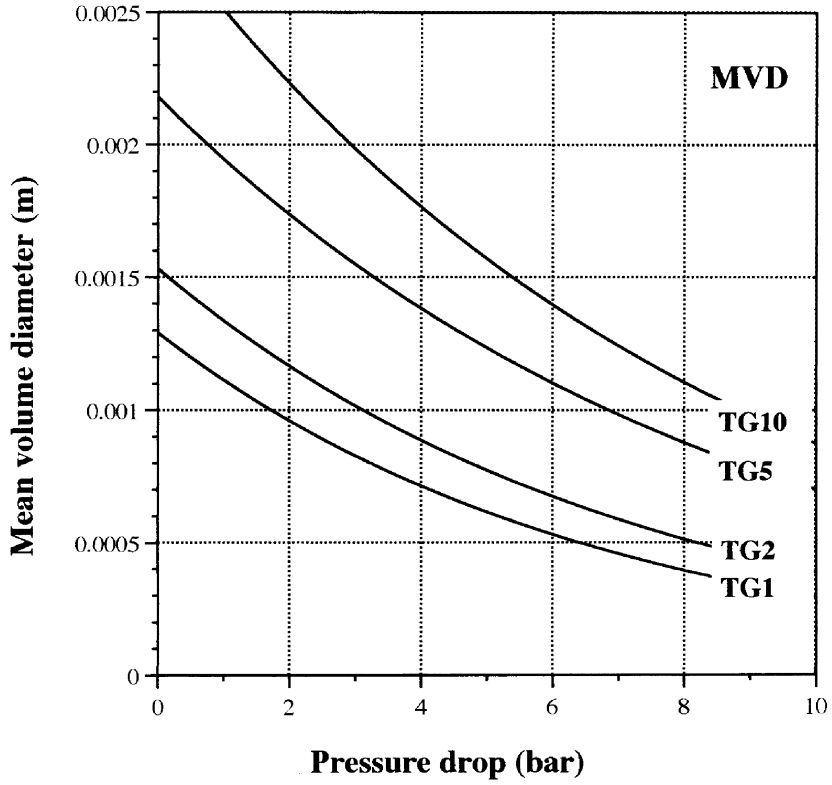


Fig. 5. Mean volume diameter of the droplets as a function of pressure drop for all nozzles (based on data provided by the manufacturer).

attained, the target was rapidly moved out of the heated region and a fast-action spherical valve was simultaneously opened on the water circuit, thus allowing two identical sprays to hit both surfaces of the target. The use of a symmetric target and of symmetric cooling by twin sprays allows one to assume symmetry, i.e., null heat flux conditions in the midplane during the temperature transient, thus making the value of the contact resistance between the two slabs immaterial and simplifying the following analysis (see below).

In all the present tests, the nozzle-target distance $X$ was 50 mm. The water was kept at ambient temperature ($\sim 20^{\circ}C$) in the pressure vessel, and a small amount of water (insufficient to create a proper spray cone) was allowed to flow out of the nozzles also in the target heat-up phase in order to cool the part of the circuit lying within the heating box, thus preventing significant variations in the exit temperature of the sprays.

During the cooling transient, the central temperature of the target was recorded by a high speed LAB–NB A/D converter, manufactured by National Instruments, connected to a Macintosh-IIx computer. Acquisition was controlled by the NI LAB-VIEW package. The interval between readings varied from 0.5 to 1.25 ms, so that the entire transient (whose duration ranged from $\sim 0.4$ to $\sim 1$ s) was described in all cases by 800 points. An independent thin-foil thermocouple, exposed to the spray in the close proximity of the target, was used to trigger the acquisition startup at the arrival of the first droplets.

## 4. Data smoothing and analysis

'Raw' recordings of the central temperature of the target during the cooling transients are reported in Fig. 7 for all nozzles and pressure drops of 2, 4 and 8 bar.

As shown in Fig. 8 (which is an enlargement of the initial part of the thermal story recorded for nozzle TG5 at $\Delta p = 2$ bar), raw data are affected by fluctuations which may include truly random noise and interferences from the 50 Hz grid supply. Thus, independent of the specific mathematical technique used in the following analysis, some smoothing of the data is required if the numerical computation of first- or higher-order derivatives has to be performed.

Three alternative smoothing techniques were tested: a simple nine-point running average, a Gaussian filter with width $\sigma = 3$ intervals between consecutive data, and a more sophisticated smooth-spline technique implemented in the computer package MATHLAB.

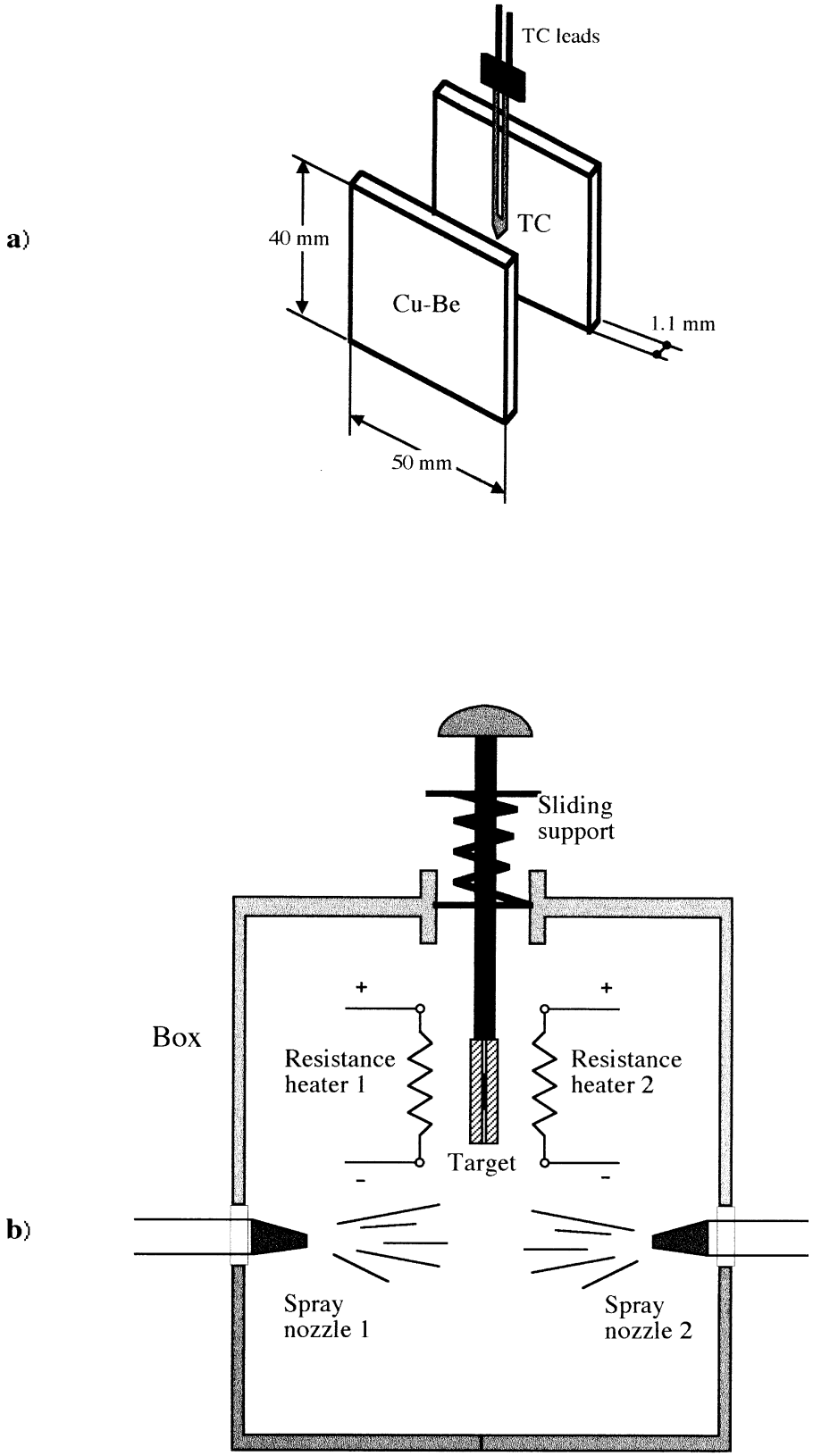


Fig. 6. Experimental setup for the heat transfer measurements: (a) schematic of the target with a thin-foil thermocouple; (b) twin-nozzle device used for the spray cooling tests.

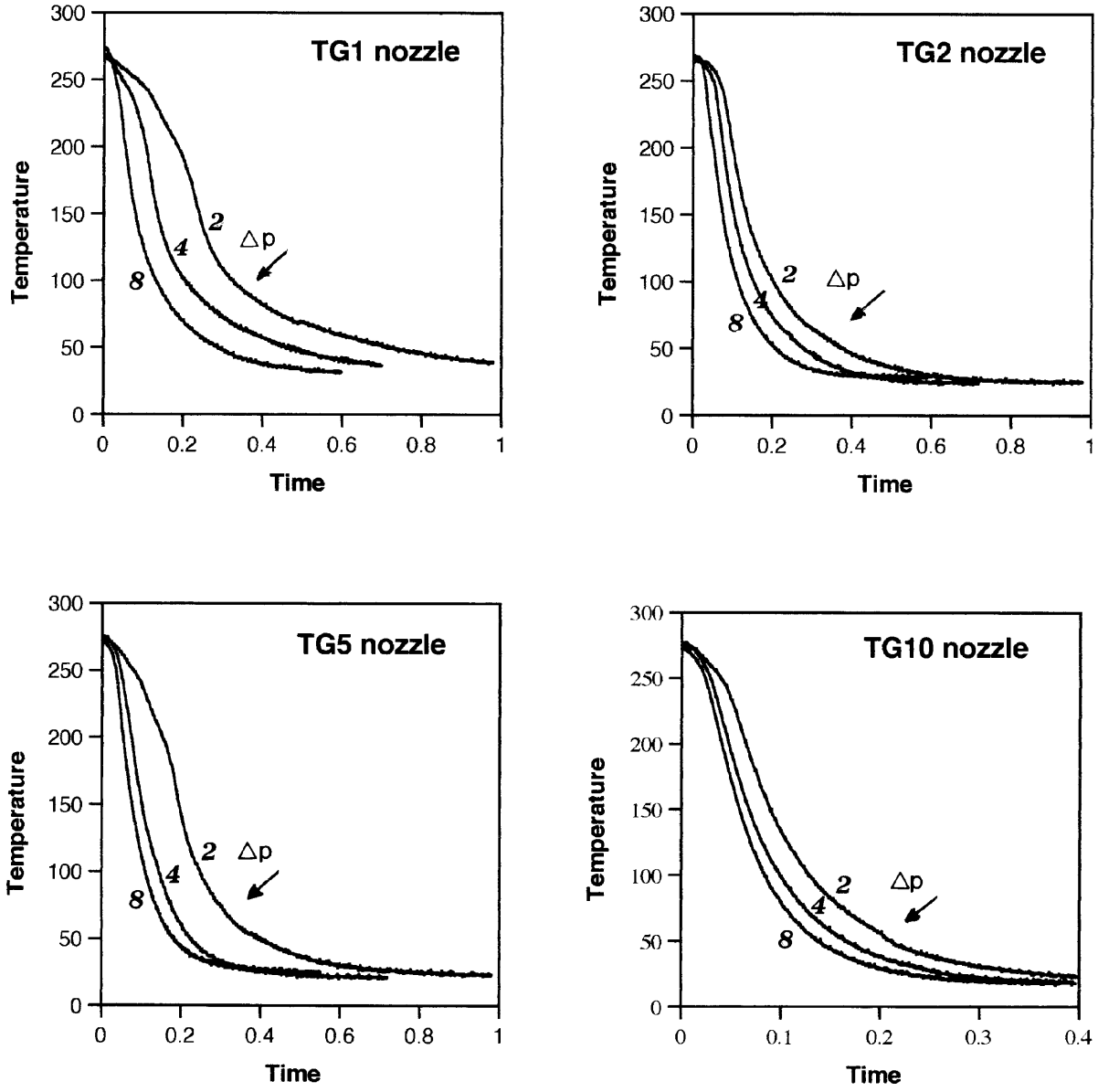


Fig. 7. Midplane temperatures recorded for all nozzles and three values of $\Delta p$ (2, 4 and 8 bar) during the cooling tests.

Figure 8 compares the 'raw' time series with the smooth curves corresponding to the three above techniques. Nine-point averaging and Gaussian filtering yield very similar results, while the smooth-spline curve, although more regular in look, tends to depart excessively from the experimental points, and thus is likely to smooth away not only noise, but also physically meaningful features of the cooling curves. For this reason, which will be better clarified later, the Gaussian filtering technique was preferred.

Once the 'raw' experimental data on the central temperature of the target have been replaced by the smooth approximation $y(t)$, an inverse heat conduction problem can be formulated, in that the wall temperature $T_w$ and the wall heat flux $q_w$ have to be determined from a knowledge of the central (smoothed) temperature $y(t)$ and, of course, of the initial conditions. Inverse problems have received considerable attention due to their ubiquitous occurrence in experimental heat transfer research, and a number of numerical techniques for their solution have

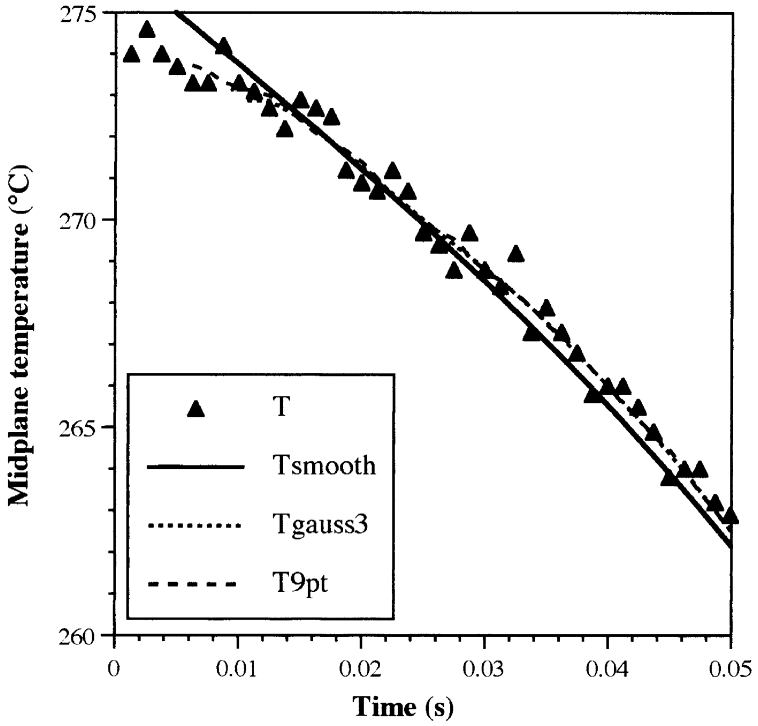


Fig. 8. 'Raw' experimental midplane temperature and continuous curves obtained by using three alternative smoothing techniques: see text for details (nozzle TG5, $\Delta p = 2$ bar).

been presented in the literature [13, 14]. In the present case the geometry of the problem is simple enough for an analytical, formally exact, solution to exist.

In fact, by neglecting the time lag between the thin-foil, Teflon-wrapped thermocouple and the surrounding material (copper), treating the problem as one-dimensional (see sketch in Fig. 9), and limiting the following analysis to the right half of the slab (positive values of $x$) for symmetry reasons, the transient heat conduction equation reduces to:

$$\frac{\partial T}{\partial x} = \alpha \frac{\partial^2 T}{\partial x^2} \tag{3}$$

with boundary conditions:

$$\left(\frac{\partial T}{\partial x}\right)_0 = 0; \tag{4}$$

$$T(0,t) = y(t) \tag{5}$$

both imposed at the midplane $x = 0$, and initial conditions:

$$T(x,0) = T^0 \text{ (uniform)} \tag{6}$$

The unknown quantities to be computed are:

$$T_w(t) = T(\delta,t) \tag{7}$$

(instantaneous wall temperature), and

$$q_w(t) = -\lambda \left(\frac{\partial T}{\partial x}\right)_\delta \tag{8}$$

(instantaneous wall heat flux), from which the cooling curve $q_w = f(T_w - T_f)$ can be obtained.

The inverse heat conduction problem in the slab, for the case of constant $\alpha$, was given a formal analytical solution as early as in 1889 by Stefan [15]. For the present configuration, Stefan's solution reduces to:

$$T(x,t) = y(t) + \sum_{n=1}^{\infty} \frac{1}{(2n)!} \frac{x^{2n}}{\alpha^n} \frac{\mathrm{d}^n y}{\mathrm{d}t^n} \tag{9}$$

for which, in particular, one has:

$$T_w(t) = y(t) + \frac{1}{2}\tau \frac{\mathrm{d}y}{\mathrm{d}t} + \frac{1}{24}\tau^2 \frac{\mathrm{d}^2 y}{\mathrm{d}t^2} + \ldots \tag{10}$$

$$q_w(t) = -\frac{\lambda_s}{\delta}\left\{\tau \frac{\mathrm{d}y}{\mathrm{d}t} + \frac{1}{6}\tau^2 \frac{\mathrm{d}^2 y}{\mathrm{d}t^2} + \ldots\right\} \tag{11}$$

where $\tau = \delta^2/\alpha$ is proportional to the conductive time constant of the slab.

Although eqns (10) and (11) are formally exact solutions of the inverse heat conduction problem, they are of limited applicability since higher-order derivatives of data affected by noise and experimental uncertainties are

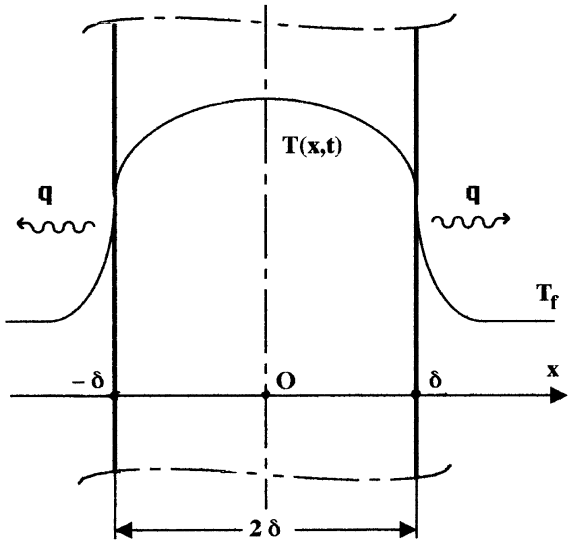


Fig. 9. Inverse heat conduction problem for the slab: sketch of one-dimensional model with convective boundary conditions.

hard to evaluate (even if the best available smoothing techniques are employed). Fortunately, both series converge rapidly and, in most cases, it is sufficient to truncate them to just a few terms.

This is shown in Fig. 10, which refers to nozzle TG1 and $\Delta p = 4$ bar; the smoothed midplane temperature $y(t)$, which is also the zeroth order approximation for $T_w$ in eqn (10), is compared with the corresponding first and second order approximations. Clearly, under the present conditions the term containing the first derivative $dy/dt$ is significant (up to $\sim 30^\circ$C for the case shown) and thus cannot be neglected, coherently with the fact that the Biot number is not much less than 1. The inclusion of the term in $d^2y/dt^2$ yields only a further correction of only $\sim 1^\circ$C, as shown in the enlargement of a small tract of the curves in graph (b), and thus can be safely omitted.

Similarly, the term containing the second derivative of $y(t)$ in eqn (11) results only in a minor contribution to the wall heat flux and can be neglected. Therefore, in analyzing the experimental data only the first two terms of eqn (10) for $T_w$ and the first term of eqn (11) for $q_w$ were retained.

Figure 11 compares the wall heat flux/wall temperature characteristic curves obtained by the above procedure for the same test case (TG5, 2 bar) using the three alternative smoothing algorithms discussed earlier. Clearly, the smooth-spline technique leads to an excessively featureless curve and to a considerable reduction of the maximum heat flux. The other two techniques yield characteristic curves which maintain the same basic features; however, the simple nine-point averaging leaves too much noise in the data, while this is canceled more effectively by Gaussian filtering. This justifies why the last technique was preferred for the subsequent analysis of the experimental data.

## 5. Wall heat transfer—wall temperature curves

During the very first instants of the cooling transient, until the hot wall has been completely wetted by the droplets, the hydrodynamic impact conditions are clearly not fully developed. Therefore, the corresponding data were excluded from the subsequent analysis. This initial 'dead period' was arbitrarily identified with the time

$$t_D = \rho D/G \tag{12}$$

that would be required for a water layer having a thickness equal to the droplet diameter $D$ to be deposited on the wall if one could neglect vaporization, rebound and fall under gravity.

The 'dead period' given by eqn (12) depended on the test conditions and, for each nozzle, was larger for lower upstream pressures (yielding larger drops and smaller flow rates). In the range examined, $t_D$ varied between $\sim 12.5$ ms (nozzle TG10 at $\Delta p = 8$ bar, with $D \approx 1$ mm and $G \approx 80$ kg m$^{-2}$ s$^{-1}$) and $\sim 100$ ms (nozzle TG1 at $\Delta p = 2$ bar, with $D \approx 1$ mm and $G \approx 10$ kg m$^{-2}$ s$^{-1}$).

Curves reporting the wall heat flux $q_w$ as a function of the wall temperature $T_w$, both quantities being computed from the 'raw' experimental data by the smoothing and inverse conduction algorithms discussed in the previous Section, are reported for all four nozzles and different values of $\Delta p$ (2, 4 and 8 bar) in Fig. 12.

These cooling curves share a number of noteworthy features. They all exhibit a broad maximum, ranging from $\sim 4$–$\sim 12 \times 10^7$ W m$^{-2}$ according to the nozzle and to the pressure drop across it, which is attained for a wall temperature of 130–170°C. Also, all curves exhibit an almost linear tract ($q_w$ proportional to $T_w - T_f$) for temperatures below $\sim 100^\circ$C, i.e., under single-phase convective conditions.

Of particular interest are the following quantities:

- the maximum, or critical, heat flux $q_c$, theoretically corresponding to the condition of departure from nucleate boiling, and the associated wall temperature $T_{DNB}$;
- the heat transfer coefficient $h$, i.e., the ratio of $q_w$ to $T_w - T_f$, in the single-phase heat transfer region ($T_w < T_{sat} + \Delta T_{sat}$, $\Delta T_{sat}$ being an appropriate wall superheat).

In principle, these quantities can be graphically derived from each cooling curve as shown in Fig. 13, which is relative to nozzle TG2 and $\Delta p = 4$ bar. However, a problem arises in deriving the single-phase heat transfer coefficient $h$ because of the residual oscillations, clearly visible in Figs 12 and 13, which the smoothing procedure is not able to eliminate, especially in the low-temperature

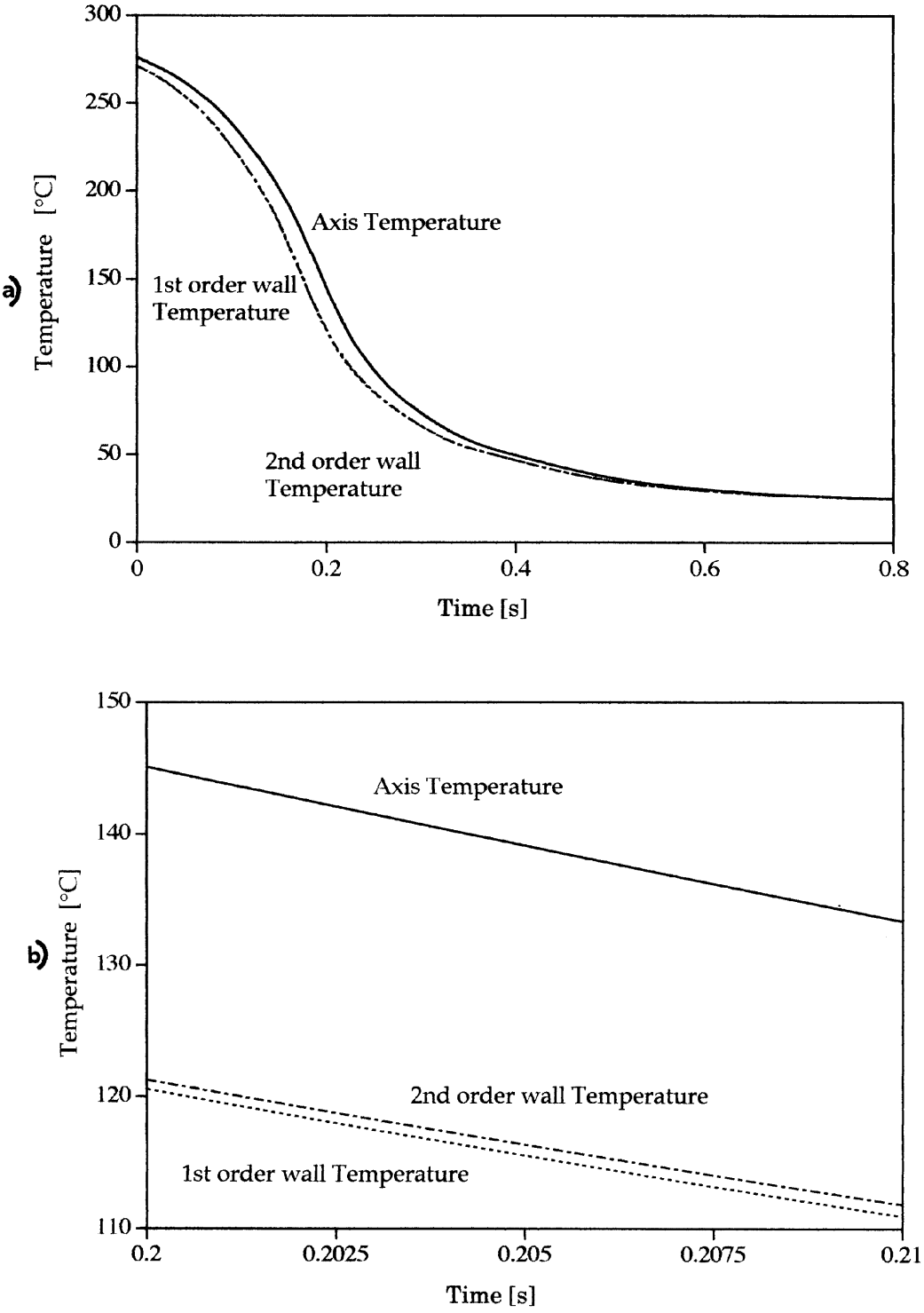


Fig. 10. Inverse heat conduction problem for the slab: comparison of successive approximations to the exact solution for the wall temperature (nozzle TG1, $\Delta p = 4$ bar). (a) overall cooling transient; (b) detail of the interval $t = 0.20$–$0.21$ s.

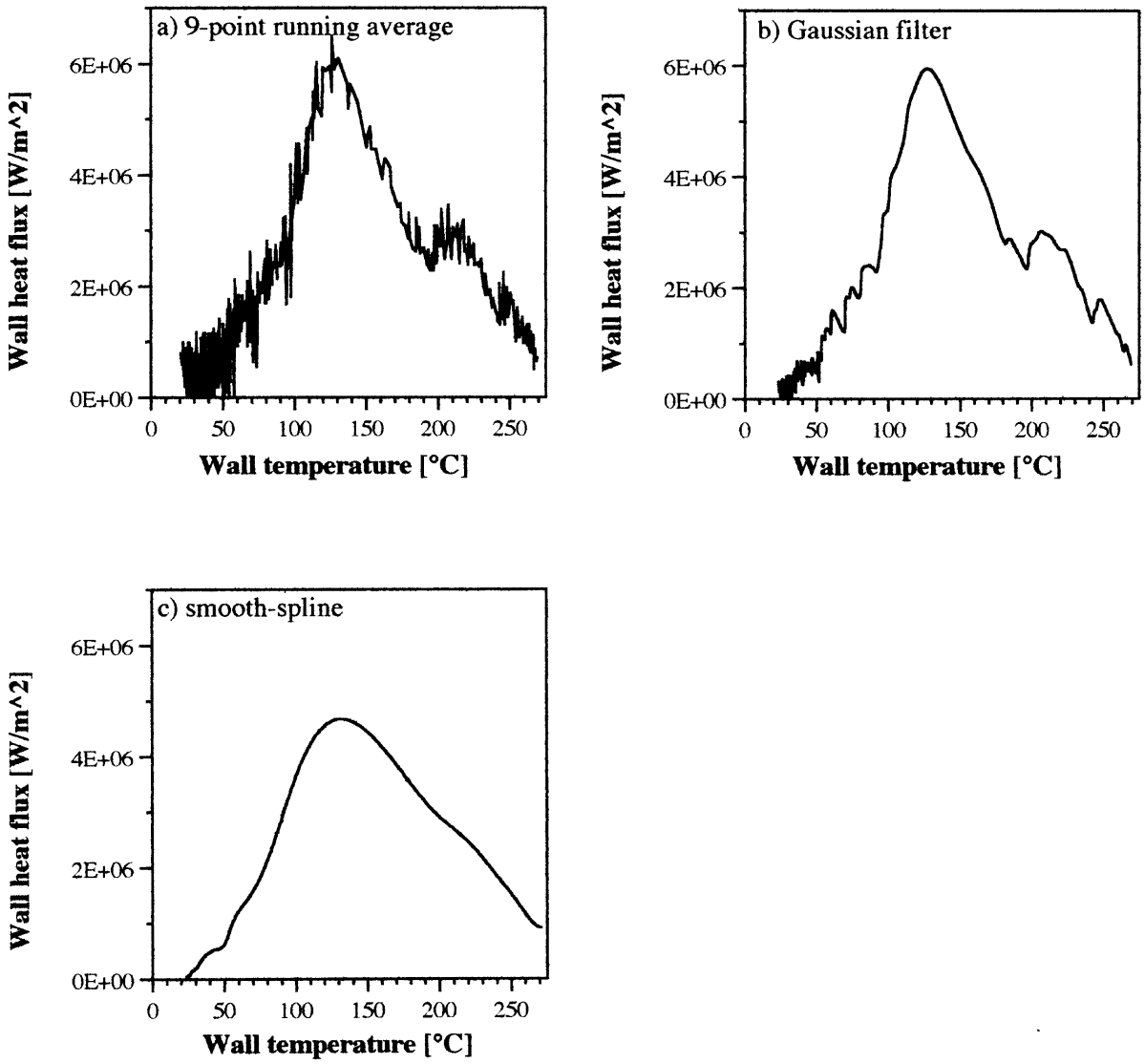


Fig. 11. Wall temperature/wall heat flux curves obtained from the data in Fig. 8 by using three alternative smoothing techniques (nozzle TG5, $\Delta p = 2$ bar).

range of the cooling curves. Noise is large in this region because the numerical derivation errors in the computed wall heat flux, eqn (12), become relatively larger when the (smoothed) midplane temperature $y(t)$ approaches its asymptotic value $T_f$.

Therefore, an alternative method was used to compute $h$. It is based on the fact that the exact solution for the midplane temperature in a slab during transient cooling at constant Biot number [12] can be approximated to a very accurate extent by the single exponential:

$$T = T_f + (T^* - T_f) \exp - \frac{t - t^*}{\tau^*} \tag{13}$$

in which the overall cooling time constant $\tau^*$ is related to the intrinsic (conductive) time constant $\tau = \delta^2/\alpha$ by $\tau^* = (0.38 + Bi^{-1})\ \tau$. In eqn (13) $t^*$ is the time at which cooling begins, $T^*$ is the (uniform) temperature of the slab at time $t^*$ and $T_f$ is the (constant) temperature of the cooling fluid.

Therefore, if the experimental (smoothed) tem-

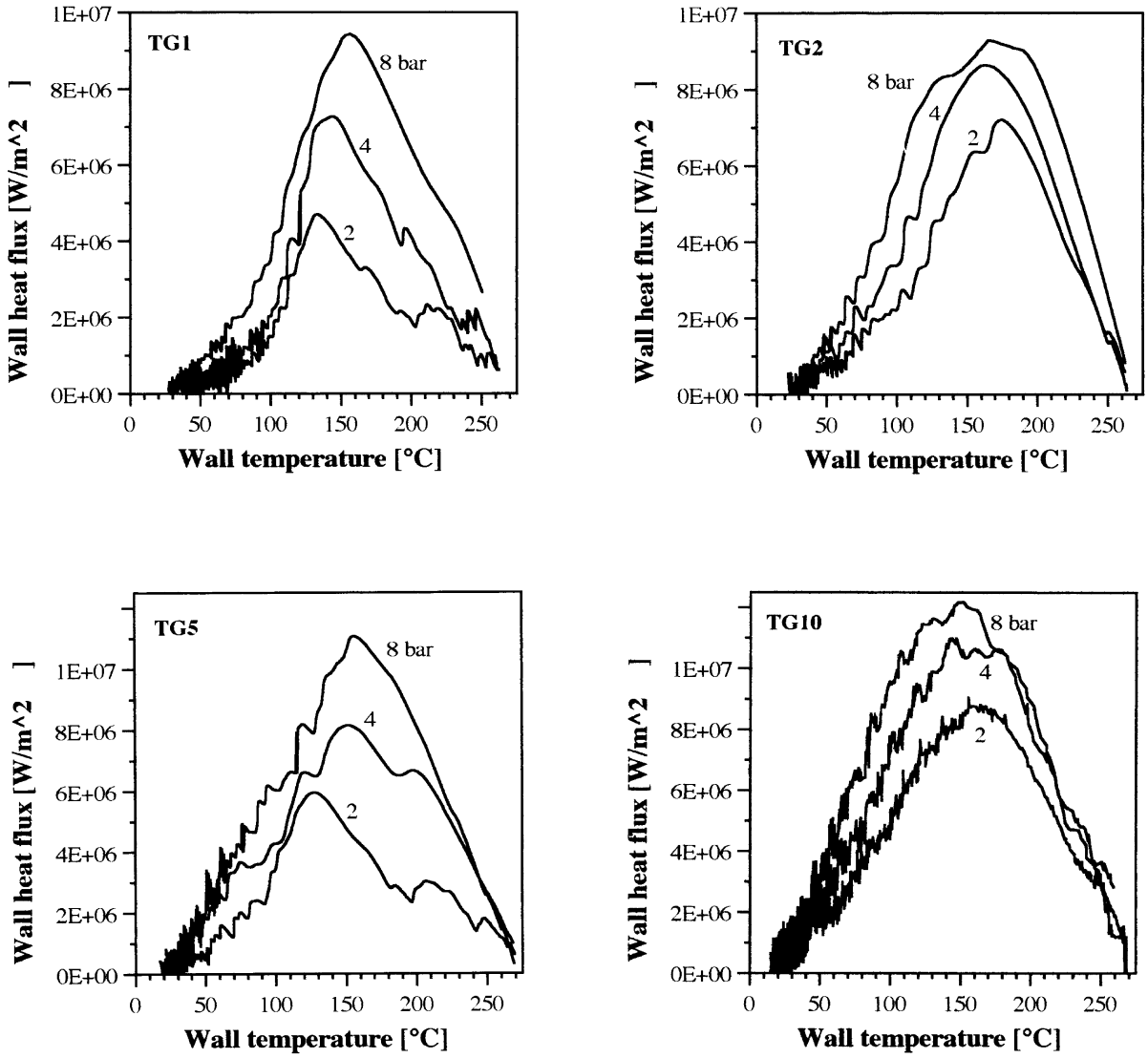


Fig. 12. Wall temperature/wall heat flux curves obtained by using the Gaussian filter for all nozzles and three values of $\Delta p$ (2, 4 and 8 bar).

peratures $y(t)$ obtained in the single-phase heat transfer region are best-fitted by an exponential of the form (13), with $\tau^*$ as the only 'free' parameter, the Biot number can then be computed as:

$$Bi = \frac{\tau}{\tau^* - 0.38\tau} \tag{14}$$

from which $h = Bi\ \lambda_s/\delta$.

The above procedure was applied choosing as the instant $t^*$ that for which the wall temperature $T_w$, computed from the smoothed experimental series $y(t)$ via eqn (10), crossed the saturation temperature of 100°C. Of course, the value of $y(t)$ for $t = t^*$ was used as the temperature $T^*$.

The cooling time constant $\tau^*$ can be determined most easily if $y(t) - T_f$ is plotted against time in semi-logarithmic form; an example is given in Fig. 14 for the two extreme cases of nozzle TG1 at $\Delta p = 2$ bar and nozzle TG10 at $\Delta p = 8$ bar.

A questionable approximation is that eqn (13) holds for an initially uniform temperature of the slab, while in the present case single-phase heat transfer begins after a rapid cooling with boiling heat transfer, so that the solid's temperature is far from uniform at that instant. However, it can be shown that the associated error is of the order

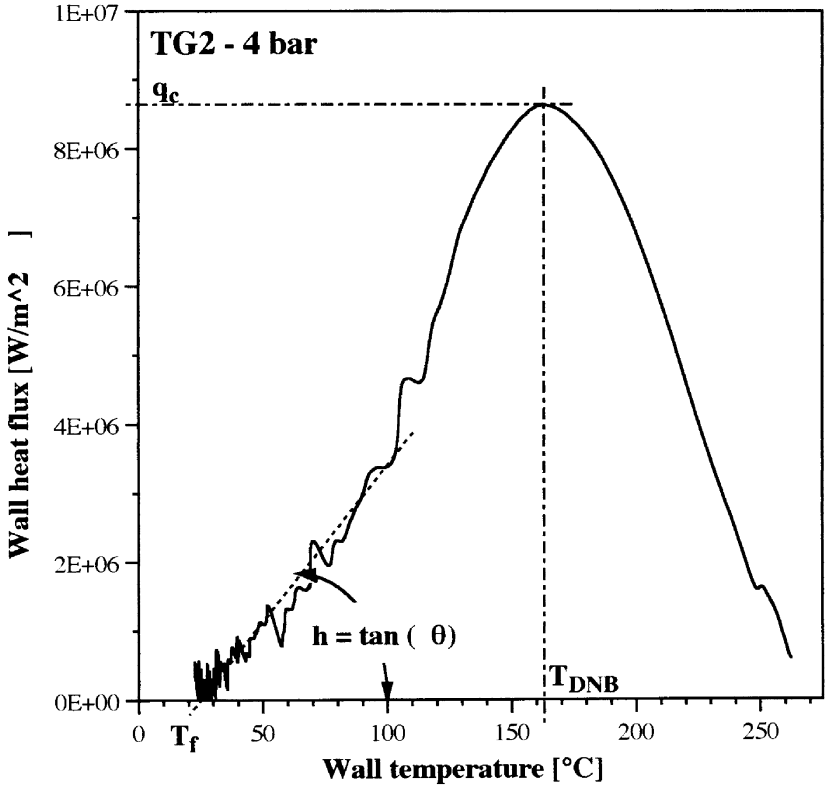


Fig. 13. Sketch of the method which can be used to derive the three quantities $h$ (single-phase heat transfer coefficient), $q_c$ (maximum, or critical, heat flux) and $T_{DNB}$ (associated temperature, or departure from nucleate boiling) from curves like those in Fig. 12 (nozzle TG2, $\Delta p = 4$ bar).

of $d^2T/dt^2$ and thus, as remarked in discussing eqns (10) and (11), is negligibly small.

## 6. Results, correlation and discussion

The resulting values of $h$, $q_c$, and $T_{DNB}$ can now be correlated with the relevant hydrodynamic characteristics of the sprays. On the basis of dimensional analysis and simple physical considerations, heat transfer was assumed here to depend only on the hydrodynamic parameters $G$, $U$ and $D$ (all defined in the previous sections). The liquid subcooling was not made to vary in the present tests and its influence was not investigated.

It should be observed that it is appropriate here to correlate heat transfer with the specific mass flow rate at the centre of the impingement area, $G$, rather than with the surface- or angle-averaged specific flow rate on the target. The reason is that, due to the small thickness of the target as compared with its lateral dimensions, the response of the thin-foil thermocouple is related to the heat flux attained in its immediate proximity, or, more exactly, in a 'spot of influence' having a radius $R$ such that the time constant for lateral heat conduction, $R^2/\alpha$, is of the same order of the total duration of the cooling transient, $t_{TOT}$. In the present tests, for $t_{TOT} \approx 1$ s and $\alpha = 2.92 \times 10^{-5}$ m$^2$/s, one has $R \approx 5$ mm. This confirms that it is appropriate to measure $G$ by the method described in section 2, i.e., in a central region $\sim 10^\circ$ in half-opening and at the same distance of the target (50 mm).

Figure 15 reports the single-phase heat transfer coefficient $h$ as a function of $G$ for all nozzles and all values of $\Delta p$. For each nozzle, $h$ increases monotonically and roughly linearly with $G$, as was stressed by connecting the associated points with solid lines. However, the points relative to different nozzles do not fall on a single line; for a given value of $G$, $h$ increases significantly going from the larger to the smaller nozzles, i.e., to larger values of pressure drop $\Delta p$ and mean velocity $U$ and smaller values of the droplet diameter $D$. Therefore, a significant influence of either $D$, or $U$, or both, is strongly suggested.

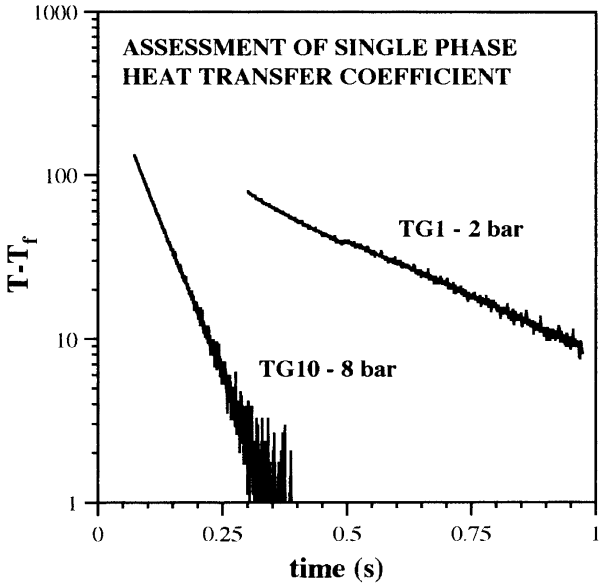


Fig. 14. Single-phase region of two typical cooling curves plotted in semi-logarithmic form in order to derive the associated time constant $\tau^*$ and the single-phase heat transfer coefficient $h$.

A least square best fit of the data with a power-law function of the form $h = CG^{\alpha}U^{\beta}D^{\gamma}$ gave the correlation:

$$h = 136G^{0.818}U^{0.871}D^{-0.066} \quad \text{(all quantities in SI units)} \tag{15a}$$

with an rms deviation of 1924 (W m$^{-2}$ K$^{-1}$), which is only a few % of the mean value of $h$.

The above values of the exponents $\alpha$, $\beta$ and $\gamma$ show that most of the nozzle-to-nozzle variation of $h$ for any given flow rate is to be attributed to the different velocity of the impinging droplets, their size playing only a minor role (which may well be a statistical artifact due to the small number and to the uncertainty of the measurement). Moreover, the close exponents of $G$ and $U$ suggest to express $h$ as a function of their product $GU$, which has the physical meaning of momentum flux on the impact surface. The resulting best-fit correlation becomes:

$$h \approx 206(GU)^{0.84} \quad \text{(all quantities in SI units)} \tag{15b}$$

for which the dispersion is only slightly higher than for eqn (15a) (rms deviation $\sim$1956 W m$^{-2}$ K$^{-1}$). Eqn (15b) was plotted in log–log form in Fig. 16; it can be seen that the results for different nozzles now collapse well near a single line. All results fall within $\pm$6% of the above correlation.

As regards the maximum wall heat flux $q_c$ (which can be identified with the critical heat flux corresponding to departure from nucleate boiling in the Nukiyama curve, see Fig. 13), overall data are reported for the various

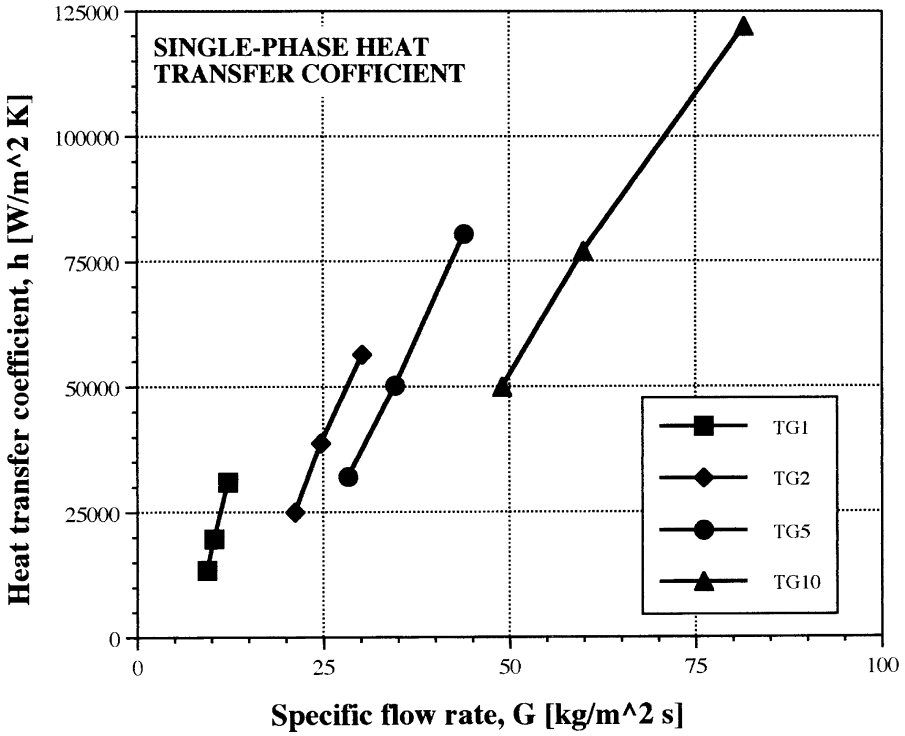


Fig. 15. Single-phase heat transfer coefficient $h$ as a function of the axial specific mass flow rate $G$ for all nozzles and all values of $\Delta p$.

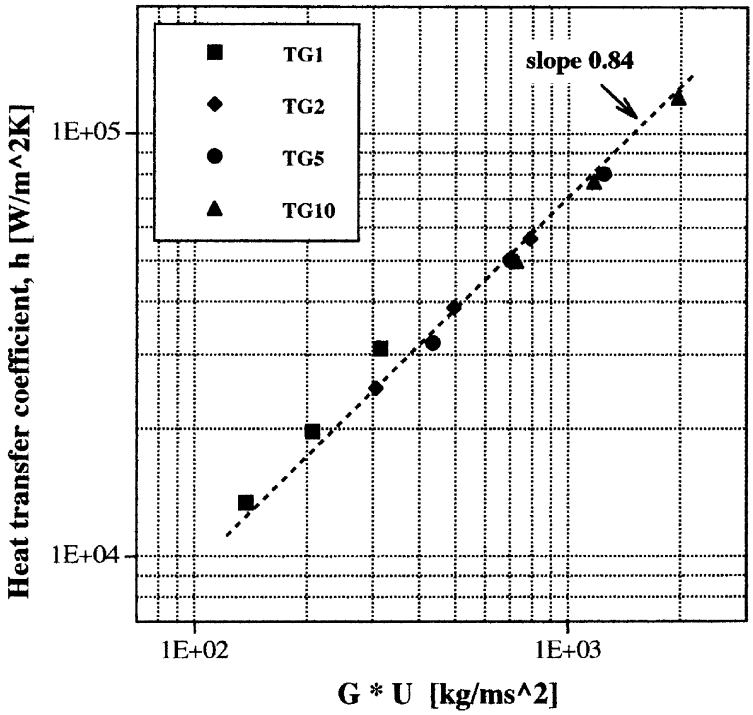


Fig. 16. Data reduction for the single-phase heat transfer coefficient $h$.

nozzles and $\Delta p$ in Fig. 17. The overall behaviour is similar to that relative to $h$, see Fig. 15; $q_c$ increases with $G$ for any given nozzle while, for a given $G$, it is larger for smaller nozzles (i.e., for smaller droplet diameters and larger droplet velocities). However, results appear far less regular than those for $h$. A least square power-law best fit using again $G$, $U$ and $D$ as the independent variables gave the correlation:

$$q_c = 0.601 \times 10^6 G^{0.26} U^{0.44} D^{-0.068}$$

(all quantities in SI units) (16a)

The root mean square deviation associated with eqn (16a) was $7.8 \times 10^5$ (W m$^{-2}$), which is about 10% of the average value of $q_c$.

The exponents of $G$ and $U$ suggest to express $q_c$ as a function of $GU^2$, which has the physical meaning of kinetic energy flux on the impact surface. Moreover, as for $h$, the overall dependence of $q_c$ on $D$ is very small and can be neglected. The following best fit correlation is thus obtained:

$$q_c \approx 0.869 \times 10^6 (GU^2)^{0.245} \quad \text{(all quantities in SI units)} \quad (16b)$$

This was represented in log–log form in Fig. 18. The data do not collapse well around a single curve as it happened for $h$; however, eqn (16b) approximates all data to within $\pm 22\%$ with an rms deviation of $\sim 8.0 \times 10^5$ (W m$^{-2}$), i.e., only slightly higher than for eqn (16a).

As regards the wall temperature at which maximum wall heat flux was obtained, corresponding to the temperature of departure from nucleate boiling (DNB) in the Nukiyama curve, no clear trend could be observed in the results, see Fig. 12, and all that can be said is that it ranged from $\sim 130$–$\sim 170$°C in all cases.

## 7. Conclusions

An experimental investigation was conducted on the cooling of hot walls by liquid water sprays by using a transient technique. Different nozzles of the swirl-spray type were tested, and attention was focussed on the nucleate boiling and single-phase heat transfer regimes. Unusually high specific mass flow rates (up to 80 kg m$^{-2}$ s$^{-1}$) were considered, yielding extremely high surface heat fluxes (above $10^7$ W m$^{-2}$) and extremely rapid temperature transients (above $10^3$°C s$^{-1}$). The choice of symmetric cooling and Gaussian smoothing of the experimental time-temperature stories recorded by a single central thin-foil thermocouple made it possible to solve the associated inverse heat conduction problem by a suit-

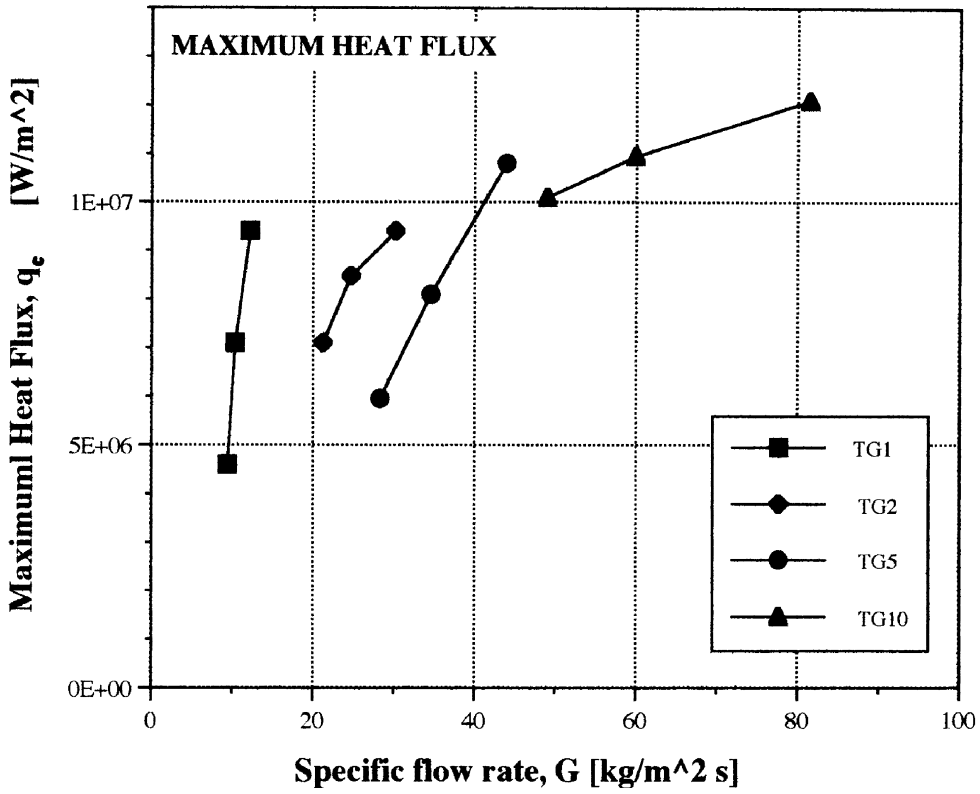


Fig. 17. Maximum wall heat flux $q_c$ as a function of the axial specific mass flow rate $G$ for all nozzles and all values of $\Delta p$.

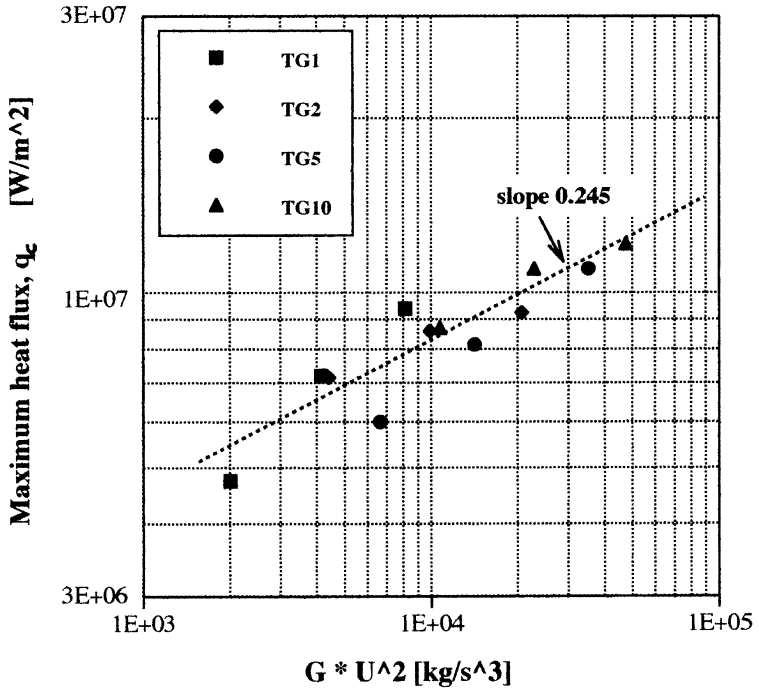


Fig. 18. Data reduction for the maximum wall heat flux $q_c$.

able truncated form of Stefan's analytical solution for the slab.

Wall temperature/wall heat flux curves thus calculated from the experimental data exhibited a clear maximum corresponding to the critical heat flux $q_c$, which was attained for wall temperatures between 130 and 170°C, and a linear region corresponding to Newtonian, single-phase heat transfer for wall temperatures below 100°C. Both the maximum heat flux $q_c$ and the single-phase heat transfer coefficient $h$ were found to correlate with the specific mass flow rate $G$ and with the mean droplet velocity $U$, while the droplet diameter $D$ had only a minor independent influence. A simple power law approximated well the experimental results for $h$, while results for $q_c$ were more scattered and less well correlated by a single simple law.

Since mass flux, drop velocity and drop diameter all vary with the pressure of the nozzle, the interdependency of these spray parameters has limited the freedom of their choice and thus the investigation of their independent effects. Therefore the results of this study, although valid for the present type of setup and within the range of parameters investigated, may not be generalized for other setups and wider ranges of conditions. Further experiments are currently in progress, in which the nozzle–target distance is made to vary thus allowing the mass flow rate to be changed without significantly altering the droplet velocity and diameter distribution. This will help to clarify the separate influence of the various spray parameters.

## Acknowledgements

The authors are grateful to Prof. S. Piccarolo for his suggestions and for the interest shown. Dott. Ing. M. Urso took part in the measurements and in the post-test analysis of the results.

## References

[1] S.-J. Chen, A.A. Tseng, Spray and jet cooling in steel rolling, Int. J. Heat and Fluid Flow 13 (1992) 358–369.

[2] M. Ghodbane, J.P. Holman, Experimental study of spray cooling with Freon-113, Int. J. Heat and Mass Transfer 34 (1991) 1163–1174.

[3] A. Yamanouchi, Effects of core spray cooling, J. Nucl. Sci. Technol. 5 (1968) 458–508 and 547–558.

[4] W.M. Grissom, F.A. Wierum, Liquid spray cooling of a heated surface, Int. J. Heat and Mass Transfer 24 (1981) 261–271.

[5] L. Bolle, J.C. Moureau, Spray cooling of hot surfaces, in: G.F. Hewitt, J.M. Delhaye and N. Zuber, (Eds.), Multiphase Science and Technology, Hemisphere, Washington, DC, 1982, pp. 1–97.

[6] K.J. Choi, S.C. Yao, Mechanisms of film boiling heat transfer of normally impacting spray, Int. J. Heat and Mass Transfer 30 (1987) 311–318.

[7] J.D. Bernardin, C.J. Stebbins, I. Mudawar, Effects of surface roughness on water droplet impact history and heat transfer regimes, Int. J. Heat and Mass Transfer 40 (1997) 73–88.

[8] J.D. Bernardin, C.J. Stebbins, I. Mudawar, Mapping of impact and heat transfer regimes of water drops impinging on a polished surface, Int. J. Heat and Mass Transfer 40 (1997) 247–267.

[9] M.L. Sawyer, S.M. Jeter, S.I. Abdel-Khalik, A critical heat flux correlation for droplet impact cooling, Int. J. Heat and Mass Transfer 40 (1997) 2123–2131.

[10] V. Brucato, S. Piccarolo, G. Titomanlio, Crystallization kinetics in relation to polymer processing, Macromol. Chemie, Macromol. Symposia 68 (1993) 245.

[11] V. Brucato, M. Ciofalo, I. Di Piazza, M.E.D. Urso, Studio sperimentale dello 'spray cooling' di pareti calde con il metodo transitorio, Dipartimento di Ingegneria Nucleare, Università di Palermo, Quaderno N.8/96, 1996.

[12] V. Isachenko, M. Osipova, A. Sukomel, Heat Transfer, MIR Publishers, Moscow, 1974.

[13] J. Taler, Theory of transient experimental techniques for surface heat transfer, Int. J. Heat Mass Transfer 39 (1996) 3733–3748.

[14] C.F. Weber, Analysis and solutions of the ill-posed inverse heat conduction problem, Int. J. Heat and Mass Transfer 24 (1981) 1783–1792.

[15] J. Stefan, Über die Theorie der Eisbildung insbesondere über Eisbildung im Polarmeere, Sitzungsberichte der Kaiserlichen Akademie Wiss. Wien, Math. Natur. 98 (1889) 965–983.